

Article

Control of Molecular Orientation and Carrier Transport of Thiophene-Based Semiconducting Polymer via Superparamagnetic Nanoparticles Fe₃O₄@C-Assisted Magnetic Alignment Method

Di Hui ¹, Tian Li ^{2,*}, Chun Ye ^{2,*} and Guoxing Pan ^{1,*}

¹ Institutes of Physical Science and Information Technology, Anhui University, Hefei 230601, China; huidi021@163.com

² Anhui Province Key Laboratory of Condensed Matter Physics at Extreme Conditions, High Magnetic Field Laboratory (HMFL), Chinese Academy of Sciences, Hefei 230031, China

* Correspondence: tianli@hmfl.ac.cn (T.L.); cye927@hmfl.ac.cn (C.Y.); pangrady@mail.ustc.edu.cn (G.P.)

Abstract: Realizing the high molecular orientation and structurally ordered microstructure of organic semiconductor polymer thin films is beneficial for enhancing the charge transport of conjugated polymers and achieving high-performance organic electronic devices. In this work, we successfully developed large-area highly aligned films of a thiophene-based polymer, namely poly(2,5-bis(3-alkylthiophen-2-yl)thieno [3,2-b] thiophene) (PBTTT), using the magnetic alignment method at a low magnetic field (0.12 T), which was assisted by superparamagnetic nanoparticles Fe₃O₄@C. The aligned microstructure of the composite films is confirmed by systematic analysis that includes polarized optical microscopy, polarized UV–visible absorption spectroscopy, and an atomic force microscope. Organic field effect transistors based on magnetic aligned composite film exhibit a 2.8-fold improvement in carrier mobility compared with the unaligned films. We hold a formation mechanism that the rapid magnetically induced self-assembly property of Fe₃O₄@C and its intermolecular interaction with polymer chains are key to the new method of preparing oriented thin films.

Keywords: magnetic alignment; semiconducting polymer; Fe₃O₄@C; composite film; OFET; hole mobility



Citation: Hui, D.; Li, T.; Ye, C.; Pan, G. Control of Molecular Orientation and Carrier Transport of Thiophene-Based Semiconducting Polymer via Superparamagnetic Nanoparticles Fe₃O₄@C-Assisted Magnetic Alignment Method. *Magnetochemistry* **2022**, *8*, 64. <https://doi.org/10.3390/magnetochemistry8060064>

Academic Editors: Hiromasa Goto, Lin Hu and Qianwang Chen

Received: 20 May 2022

Accepted: 7 June 2022

Published: 10 June 2022

Publisher's Note: MDPI stays neutral with regard to jurisdictional claims in published maps and institutional affiliations.



Copyright: © 2022 by the authors. Licensee MDPI, Basel, Switzerland. This article is an open access article distributed under the terms and conditions of the Creative Commons Attribution (CC BY) license (<https://creativecommons.org/licenses/by/4.0/>).

1. Introduction

Conjugated polymers are of great interest for a variety of applications, including organic field effect transistors [1,2], organic light-emitting diodes [3,4], and organic photovoltaic cells [5,6], owing to their low temperature, solution processability, and mechanical flexibility, which may enable the fabrication of low-cost and large-area flexible electronic devices. However, most semiconductor polymer-based devices suffer from a low performance, which leads to their limitation in a wide range of applications.

It is already well-established that the charge mobilities are highest along the backbone chain and the π - π stacking directions, but low along the alkyl side chain direction [1,7–9]. Therefore, a key method for improving the charge transport of semiconductor polymers is to align the main chains of the semiconducting polymers [8–10]. Aligned films not only enhance the mobilities along the preferred backbone direction, but also provide a unique opportunity to study the interaction between polymer film microstructure and charge transport performance.

So far, several facile and efficient methods to realize oriented polymer thin films have been reported, such as off-center spin coating [11,12], bar coating [13,14], shear coating [15], Chinese brush coating [8], dip coating [1,16], and electric field alignment [17,18]. In addition to these techniques, the magnetic alignment method acts as a tool for tuning molecular

alignment for the fabrication of a large-area aligned film in a clean (non-contact) manner, which is more suitable for device applications.

In general, the anisotropy of the magnetic susceptibility of molecules causes anisotropy of the molecular magnetic energy, which leads to magnetic alignment [19–22]. Nevertheless, mostly conjugated polymers are diamagnetic materials, and their magnitude is typically on the order of -10^{-8} to -10^{-6} [22–24]. Thus, a high magnetic field (>6 T) is usually required to achieve magnetic alignment of polymer molecules [24–27]. Therefore, a high magnetic field of 45 T was used to align carbon nanotubes [25]. Our previous work demonstrated that the semiconducting polymers of P(NDI2OD-T2) and PBTTT can be aligned to a high degree under an 8 T high magnetic field [26,27]. Due to the limitation of high-magnetic-field conditions, the practical application of organic semiconductor polymer growth and structure regulation under a magnetic field has been largely limited. Thus, developing a facile approach that enables the alignment of polymer chains on a large area by using a smaller magnetic field is urgently needed for its practical application.

Smaller magnetic fields have been used to align nonmagnetic microparticles, but only with the assistance of magnetic or superparamagnetic nanoparticles [28–30]. This method was previously used to align carbon nanotubes and graphene flakes with a low magnetic field in the range 0.1 to 0.8 T [29–32]. This is mainly due to van der Waals forces, as the Fe_3O_4 nanoparticles can easily attach to the surface of carbon nanotubes and graphene flakes to make them more responsive to a magnetic field. However, polymer molecules have difficulty in forming strong interactions with Fe_3O_4 nanoparticles. Thus, examples of a low-magnetic-field manipulation of the film structure of polymer/ Fe_3O_4 nanohybrids are scarce.

In this work, we report a simple, novel and upscalable method to form a well-oriented poly(2,5-bis(3-alkylthiophen-2-yl)thieno [3,2-b] thiophene) (PBTTT) thin film by applying a low magnetic field (0.12 T) assisted by carbon-encapsulated Fe_3O_4 superparamagnetic colloidal nanoparticles ($\text{Fe}_3\text{O}_4@\text{C}$). This method mainly relies on the strong response of the superparamagnetic nanoparticles to the magnetic field and the characteristics of rapid magnetically induced self-assembly, as well as a strong interaction with polymer molecules, to improve the orientation and crystallinity of low-magnetic-field-induced polymer films.

More importantly, structure and orientation were characterized by polarized light absorption spectroscopy. We found that the presence of a small amount of $\text{Fe}_3\text{O}_4@\text{C}$ nanoparticles in the weak magnetic field greatly improved the degree of chain alignment, and the chain backbones of PBTTT within the composite films are highly aligned along the direction of the applied magnetic field. Furthermore, the degree of chain alignment of the composite films is higher than that of pure polymer films aligned by a high magnetic field (8 T) [26]. We also found that such structural tuning plays a crucial role in the carrier transport of the organic field-effect transistor (OFET) devices.

2. Materials and Methods

2.1. Materials

PBTTT was purchased from 1-Material inc. and used as received. Ferrocene ($\geq 98\%$) and o-dichlorobenzene ($\geq 99\%$) was purchased from Alfa Aesar. The hydrogen peroxide ($\geq 30\%$) and acetone ($\geq 99\%$) were of analytic grade from the Shanghai Chemical Factory, China. All chemicals were used as received without further purification.

2.2. Synthesis of Monodispersed $\text{Fe}_3\text{O}_4@\text{C}$ Colloidal Nanoparticles

The synthesis followed a typical procedure, as in previous work [33,34]. Ferrocene (0.3 g) was first dissolved in acetone (30 mL) under continuous mechanical stirring for 30 min, and 1.5 mL of hydrogen peroxide was slowly added to this mixed solution, which was then mechanically stirred for 1 h. The mixture was transferred into a Teflon-lined stainless-steel autoclave with a 50 mL capacity and heated at 240 °C for 72 h. Then, the black product was washed with acetone several times to remove excess ferrocene and dried under vacuum at 50 °C for 5 h for further use.

2.3. Preparation of Fe₃O₄@C/PBTTT Composite Solution

At first, Fe₃O₄@C dispersions were prepared by the Fe₃O₄@C powder added into o-dichlorobenzene (o-DCB) with a concentration of 2 mg/mL. The mixture was then sonicated at 540 W for 30 min. After settling for 1 h, homogeneous dark Fe₃O₄@C dispersion was generated from the top portion of the solution. The PBTTT was dissolved in o-DCB to form a solution of 10 mg/mL and blended with Fe₃O₄@C dispersion at volume ratio of 10:1. The solution was then sonicated at 50 W for 10 h to yield the composite solution.

2.4. Magnetic Alignment

Alignment experiments were performed using a magnet with a 0.12 T magnetic field. The magnet was designed and manufactured by Hefei Hongzhong Science & Technology Company (Hefei, China) and is shown in Figure S1. The aligned films were prepared by casting the Fe₃O₄@C/PBTTT composite solution on the Si/SiO₂ substrates under the magnetic field at room temperature (RT). The magnetic field was applied until the solvent was evaporated. The films from the magnetic alignment process were then thermally annealed at 180 °C for 20 min in a N₂ atmosphere and then allowed to cool down to RT slowly in order to remove the remaining solvent and improve the structural order of the films.

2.5. Sample Characterization

The X-ray diffraction (XRD) patterns were collected on a Rigaku MiniFlex powder X-ray diffractometer using Cu-K α radiation ($\lambda = 1.54 \text{ \AA}$) over a 2θ range of 20°–80°. Static magnetic properties were measured with a superconducting quantum interference device (MPMS3, Quantum Design company, San Diego, CA, USA). The Fourier transform infrared (FT-IR) spectra of samples were taken on a VERTEX-80V spectrometer (Bruker Corporation, Billerica, American) in the range of 500–4000 cm⁻¹. The Raman spectrum was taken on a Horiba Jobin Yvon T64000 Micro-Raman instrument (HORIBA, Ltd., Kyoto, Japan) with the 532 nm line at room temperature. The morphology and structure of the products were analyzed by employing scanning electron microscopy (SEM, Helios NanoLab 600i, FEI Company, Hillsboro, OR, USA). Optical texture and the morphology of the prepared films were probed by a polarized optical microscope as well as a HITACHI-5500M atomic force microscope (AFM, Tokyo, Japan) in the tapping mode, respectively. The film optical anisotropy was examined by a UV-vis spectrophotometer (Shimadzu, UV-3100, Kyoto, Japan) in transmission geometry on the quartz substrates.

2.6. OFET Fabrication and Characterization

The bottom-gate/bottom-contact (BG/BC) OFET devices were fabricated on heavily doped Si wafers with a 230 nm thermally grown SiO₂ layer. The surfaces of the Si/SiO₂ substrates were photolithographically pre-patterned with inter-digitated electrode arrays of Cr/Au (3 nm/50 nm) as source/drain electrodes. The electrode arrays are characteristic of the channel width (W) of 1.7 mm and channel lengths (L) of 200 μm . The aligned Fe₃O₄@C/PBTTT composite films were prepared as previously described. The films were then thermally annealed at 180 °C for 60 min in a N₂ glove-box. The BC/BG OFETs were therefore constructed via the above procedure. The devices were characterized in a N₂ atmosphere using a Keithley 2612A parameter analyzer on a probe station. The field-effect mobility (μ_{FET}) was calculated in the saturated regime according to the transistor equation:

$$I_D = \frac{WC_i\mu_{\text{FET}}(V_G - V_T)^2}{2L}$$

where C_i is the area capacitance of dielectric (15 nF/cm² for SiO₂), V_G is the gate voltage, and V_T is the threshold voltage.

3. Results and Discussion

3.1. Microstructure of $\text{Fe}_3\text{O}_4@\text{C}$ Nanoparticles

The molecular structures of the PBTTT polymer used in this study are shown in Figure 1a. Figure 1b,c show the SEM images of $\text{Fe}_3\text{O}_4@\text{C}$ colloidal nanoparticles sample, where we can observe that the sample is composed of many nearly monodisperse spherical particles with a diameter of approximately 100 nm. The XRD pattern of the as-prepared samples is shown in Figure S2. All the diffraction peaks are in accordance with the standard profile of cubic magnetite Fe_3O_4 (JCPDS file No. 19-0629).

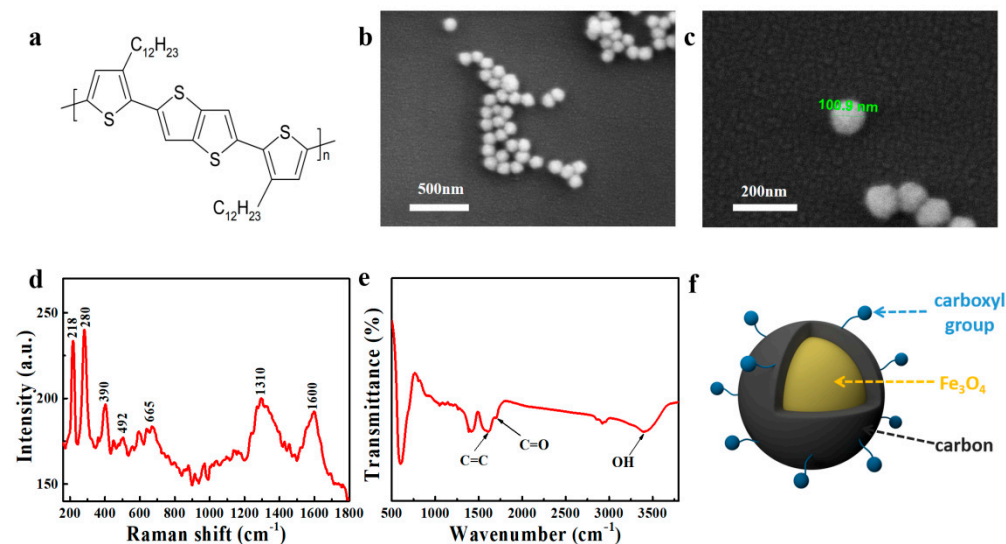


Figure 1. (a) Chemical structures of PBTTT; (b,c) SEM images of $\text{Fe}_3\text{O}_4@\text{C}$ nanoparticles; The Raman profile spectrum (d) and FT-IR spectrum (e) of $\text{Fe}_3\text{O}_4@\text{C}$ nanoparticles, respectively. (f) 3D model of $\text{Fe}_3\text{O}_4@\text{C}$ nanoparticles.

No additional peaks are observed, which suggests the high purity of the Fe_3O_4 phase [34,35]. The Raman profile spectrum of $\text{Fe}_3\text{O}_4@\text{C}$ nanoparticles (Figure 1d) exhibits two broad peaks (D-peak at 1310 cm^{-1} and G-peak at 1600 cm^{-1}), which indicate the dominant existence of a carbon phase in the samples [36]. We also performed an FT-IR spectrum analysis of the samples to further confirm the existence of carbon (Figure 1e). The two broad peaks around 1700 cm^{-1} and 3410 cm^{-1} were apparently caused by the stretching vibration of carboxyl that rose from the carboxyl groups on the surface of the nanoparticles. Thus, the nanoparticles exhibit a negative zeta potential due to the carboxyl with a negatively charged group [34,36,37].

It is worth noting that there is no peak corresponding to the carbon shell in the XRD pattern (Figure S2), which may be the carbon shell prepared by the hydrothermal method in an amorphous state. On the basis of the abovementioned measurement result, the prepared nanoparticles contain a magnetite/carbon core/shell structure with the carboxyl groups on the surface (Figure 1f), and the diameter is approximately 100 nm.

3.2. Microstructure of Magnetically Aligned Films

The magnetically aligned $\text{Fe}_3\text{O}_4@\text{C}/\text{PBTTT}$ composite films are prepared on the Si/SiO₂ substrates by solution casting from the composite solution under a permanent magnet with a magnetic field of 0.12 T at room temperature. The schematic of the fabrication procedure for the $\text{Fe}_3\text{O}_4@\text{C}/\text{PBTTT}$ composite thin film is also shown in Figure 2a. To visualize the anisotropy of the $\text{Fe}_3\text{O}_4@\text{C}/\text{PBTTT}$ composite film, the film surface is imaged by using polarized optical microscopy (POM). As shown in Figure 2b, the POM images of the magnetically aligned $\text{Fe}_3\text{O}_4@\text{C}/\text{PBTTT}$ composite film exhibit a homogeneous change in color and brightness, which indicates a uniaxial alignment of the composite film in a large-area.

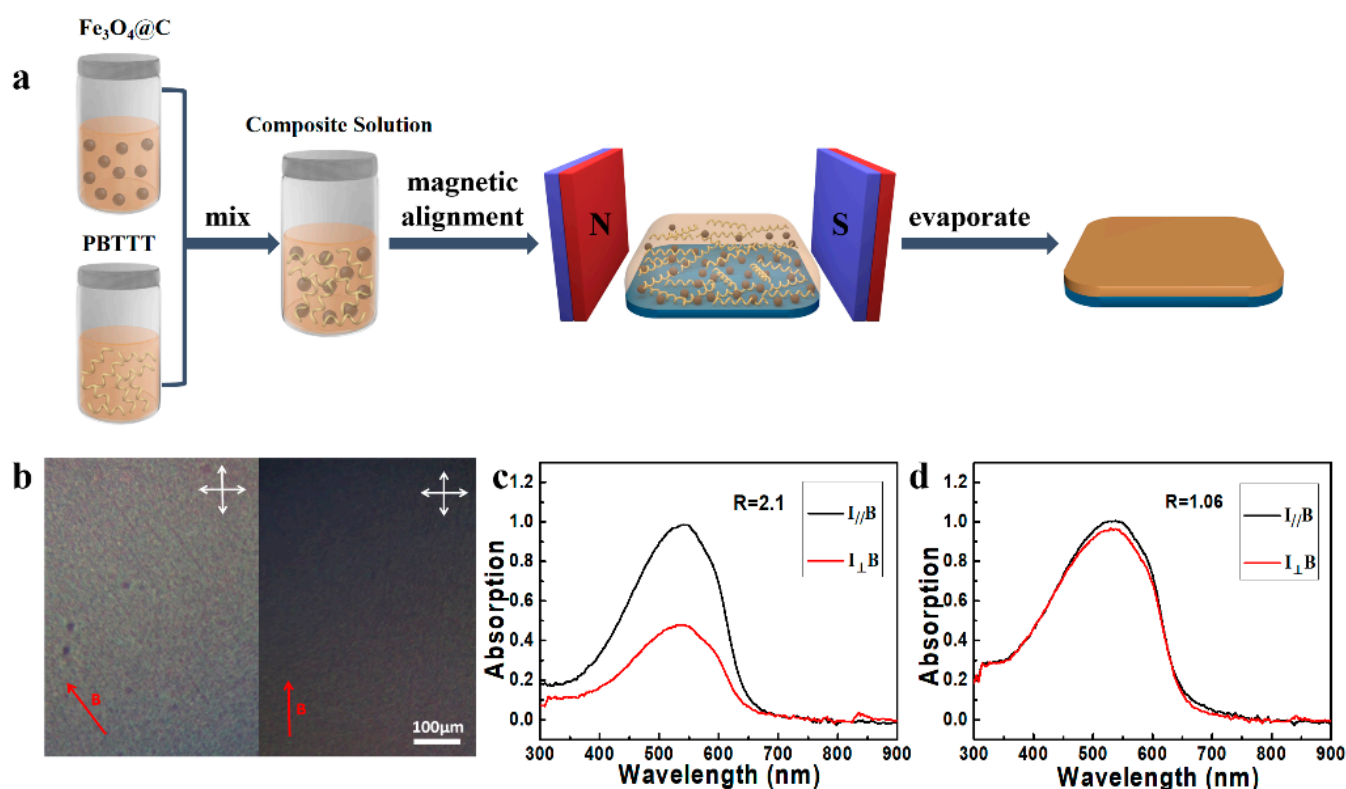


Figure 2. (a) Schematic illustration of the methodology for the formation of the composite film via magnetic alignment method; (b) The POM images of the magnetically aligned Fe₃O₄@C/PBTTT composite film. The red arrows denote the magnetic field direction; Polarized UV-vis absorption spectra of the PBTTT film, which magnetically aligned with (c) and not with (d) Fe₃O₄@C nanoparticles, respectively.

The brighter image was observed at the angle between the magnetic field direction, and the polarization axis is 45°, which clearly indicates that the direction of the PBTTT molecules backbone is oriented either parallel or perpendicular to the magnetic field direction. However, the POM images of the pure PBTTT film were magnetically aligned without Fe₃O₄@C nanoparticles, which displayed no difference regardless of the rotation of the film (Figure S3). This illustrates the isotropic texture structure of the pure PBTTT film with random distributed molecule chains. Interestingly, we should note that the superparamagnetic Fe₃O₄@C nanoparticles form micron-scale chain-like structures and are highly oriented and uniformly dispersed in the composite film. This phenomenon will be discussed in detail later.

In order to deduce the molecular chain direction of PBTTT and the degree of alignment of the composite film, polarized UV-vis absorption spectroscopy was performed. This is mainly because the transition dipole moment of polymers is typically aligned along the backbones; the orientation of the polymer backbone can be estimated by this measurement. Furthermore, the degree of alignment of the films can be quantified by the dichroic ratio of the maximum absorbance, $R = I_{\parallel} / I_{\perp}$, where I_{\parallel} and I_{\perp} denote the peak absorbance in which the applied magnetic field direction is parallel and perpendicular to the direction of incident light, respectively [1,38]. As shown in Figure 2c, the magnetically aligned Fe₃O₄@C/PBTTT composite film shows a stronger absorption at 535 nm when the direction of the applied magnetic field is parallel to the polarization direction of the incident light. This confirms that the chain backbones of PBTTT should be preferentially aligned with the magnetic field direction [38,39].

The composite film has a dichroic ratio of 2.1 at 535 nm, which is higher than that of the aligned pure PBTTT films fabricated by solution casting under 8 T (dichroic ratio = 1.6)

as previously reported by us [26]. This suggests that the $\text{Fe}_3\text{O}_4\text{@C}$ -nanoparticles-assisted low-magnetic-field alignment method is able to effectively align polymer backbones and fabricate a higher anisotropic polymer film than the film grown without the $\text{Fe}_3\text{O}_4\text{@C}$ -nanoparticles-assisted high-magnetic-field alignment method. As a comparison, the pure PBTTT film, which is magnetically aligned without $\text{Fe}_3\text{O}_4\text{@C}$ nanoparticles, exhibits a dichroic ratio of 1.06, the isotropic (unaligned) character shown in Figure 2d. This result is consistent with the POM characterization.

We further characterized the surface morphology changes in the films by the tapping-mode atomic force microscopy (AFM). As shown in Figure 3, the height images of the magnetically aligned $\text{Fe}_3\text{O}_4\text{@C}$ /PBTTT composite film exhibit the formation of fiber structures with a good alignment in the direction of the arrow that corresponds to the magnetic field direction. In contrast, the $\text{Fe}_3\text{O}_4\text{@C}$ /PBTTT composite film without magnetic alignment exhibit a disordered surface morphology with small grains.

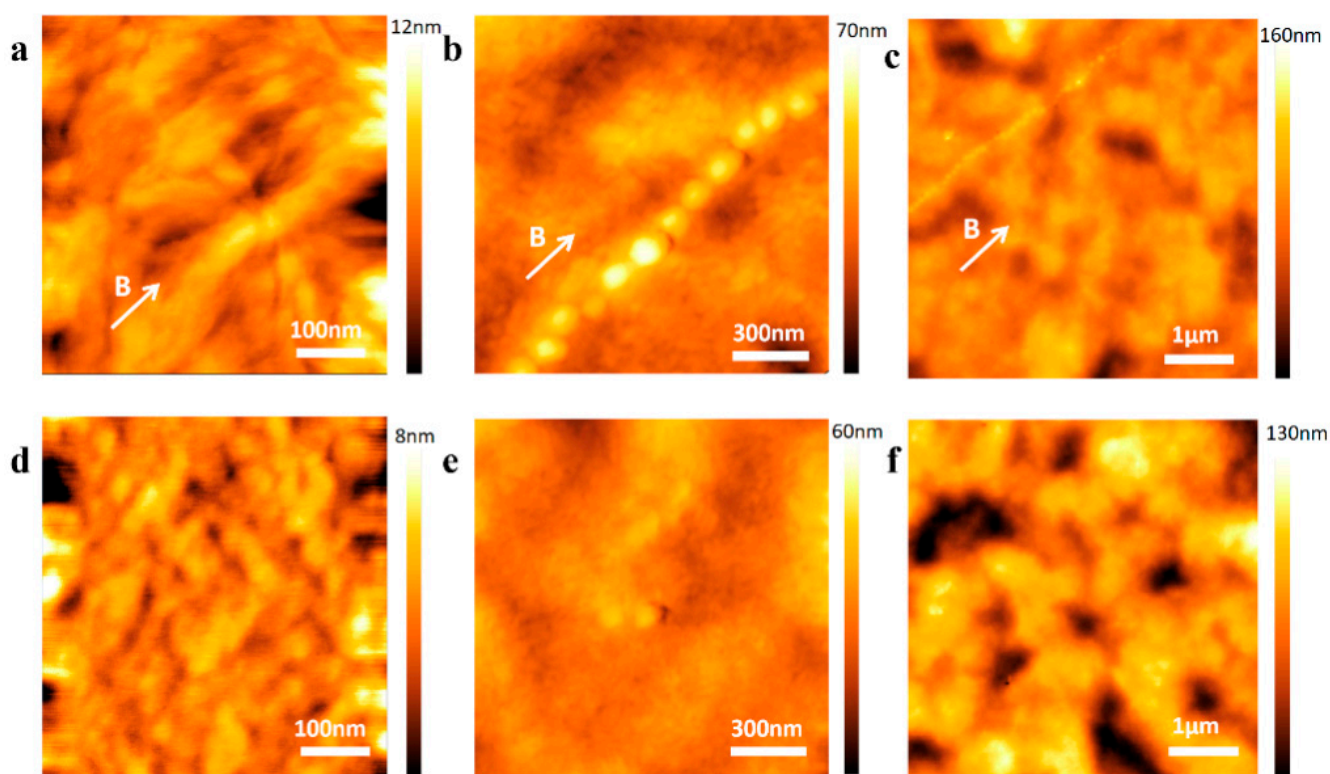


Figure 3. Tapping-mode AFM images of the $\text{Fe}_3\text{O}_4\text{@C}$ /PBTTT composite films cast with (a–c) and without magnetic field (d–f). The white arrows denote the magnetic field direction.

Taken together, the AFM images clearly indicate that the $\text{Fe}_3\text{O}_4\text{@C}$ -nanoparticles-assisted magnetic alignment method allows for a highly oriented polymer film under a low magnetic field. Compared with the disordered distribution of the $\text{Fe}_3\text{O}_4\text{@C}$ nanoparticles without magnetically aligned $\text{Fe}_3\text{O}_4\text{@C}$ /PBTTT composite films, the $\text{Fe}_3\text{O}_4\text{@C}$ nanoparticles formed chain-like structures, which are fixed inside the aligned composite film with a regular interparticle spacing under the induction of the applied low magnetic field.

3.3. Charge Transport Studies

The effect of the polymer molecule chain alignment on the charge transport properties is investigated by fabricating bottom-gate/bottom-contact (BG/BC) OFETs (Figure 4a). We define two main orientations for the OFETs: (1) parallel, where the transistor channel is parallel to the magnetic field direction ($\mu\parallel$), and (2) perpendicular, where the transistor channel is perpendicular to the magnetic field direction ($\mu\perp$). As shown in Figure 4b,c and Figure S4 in the Supporting Information, in the aligned $\text{Fe}_3\text{O}_4\text{@C}$ /PBTTT composite-film-based OFET,

the hole mobilities are measured to be $2.7 \times 10^{-2} \text{ cm}^2 \text{ V}^{-1} \text{ s}^{-1}$ and $8.3 \times 10^{-3} \text{ cm}^2 \text{ V}^{-1} \text{ s}^{-1}$ in the parallel and perpendicular directions, respectively, which leads to a ratio of about 3.2. The hole mobility in the parallel device is enhanced by a factor of 2.8 with respect to isotropic devices of unaligned pure PBTTT film ($9.5 \times 10^{-3} \text{ cm}^2 \text{ V}^{-1} \text{ s}^{-1}$).

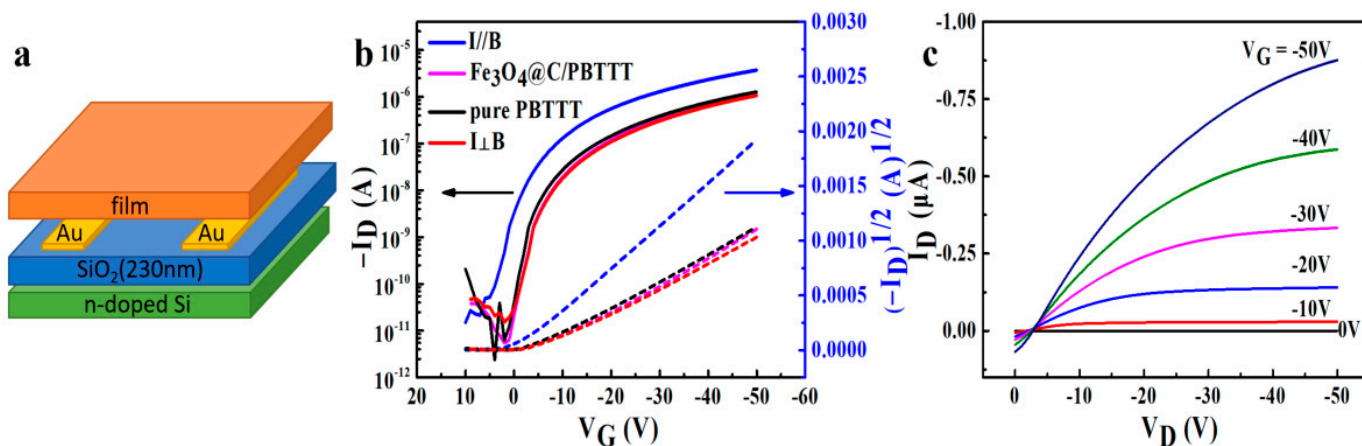


Figure 4. (a) Illustration of bottom-gate/bottom-contact (BG/BC) OFET device configuration; (b) Typical transfer characteristics for the BG/BC OFETs employing the magnetically aligned $\text{Fe}_3\text{O}_4@\text{C}/\text{PBTTT}$ composite film as well as unaligned spin-coated pure PBTTT film (black line) and spin-coated $\text{Fe}_3\text{O}_4@\text{C}/\text{PBTTT}$ composite film (pink line). The channel current is parallel ($I_{||B}$) (blue line) and perpendicular ($I_{\perp B}$) (red line) to the magnetic field direction. (c) Typical output curves of the BG/BC parallel device.

These results support the conclusion that the composite film with an induced alignment provided improved charge transport. Moreover, there is little difference in hole mobility between the unaligned $\text{Fe}_3\text{O}_4@\text{C}/\text{PBTTT}$ composite film ($9.3 \times 10^{-3} \text{ cm}^2 \text{ V}^{-1} \text{ s}^{-1}$) and pure PBTTT film-based devices, which suggests that a small amount of $\text{Fe}_3\text{O}_4@\text{C}$ nanoparticles in the composite film do not obviously affect the carrier transport. Thus, it is clear that a higher hole mobility in the aligned composite films clearly originates from the high orientation of the polymer chains. The anisotropy and significant enhancement of hole mobility for the aligned composite-film-based OFETs are mainly due to their highly aligned structural features, which favor charge transport along the preferential backbone chain direction and greatly reduce the number of slow and energy-demanding interchain hopping events from the source to the drain electrodes [15,40,41].

3.4. The Mechanism for Magnetic Alignment

To thoroughly explain the abovementioned phenomenon, we conduct further research on the alignment mechanism of the $\text{Fe}_3\text{O}_4@\text{C}$ -nanoparticles-assisted magnetic alignment method. First, the magnetic measurements are carried out on both $\text{Fe}_3\text{O}_4@\text{C}$ and PBTTT materials. Figure 5a shows the magnetization curves of PBTTT, and the diamagnetic susceptibilities of $6.5 \times 10^{-8} \text{ emu g}^{-1} \text{ Oe}^{-1}$ are obtained. Such a weak susceptibility indicates that PBTTT cannot be magnetically oriented by the low magnetic field of 0.12 T, which is confirmed by the above structural characterization. In contrast, a significant hysteresis loop in the $\text{Fe}_3\text{O}_4@\text{C}$ M-H curve reveals the superparamagnetic behavior of the $\text{Fe}_3\text{O}_4@\text{C}$ (Figure 5b). The saturation magnetization (M_s), remanent magnetization (M_r) and coercivity (H_c) values of the $\text{Fe}_3\text{O}_4@\text{C}$ at room temperature are $52 \text{ emu g}^{-1} \text{ Oe}^{-1}$, $1.4 \text{ emu g}^{-1} \text{ Oe}^{-1}$ and 25 Oe , respectively, which is in accordance with the previously report literature [34].

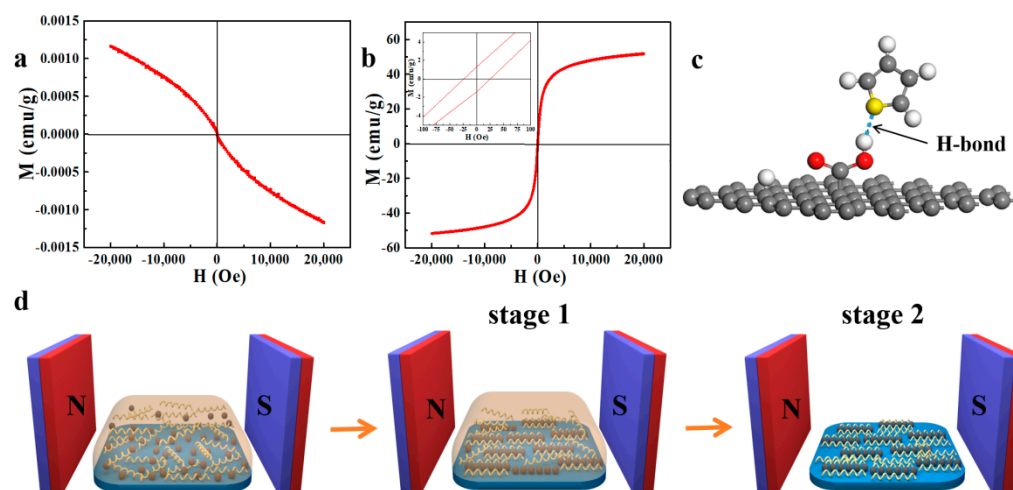


Figure 5. Magnetization versus magnetic field (M - H) curves at room temperature ($25\text{ }^{\circ}\text{C}$) of PBTTT (a) and $\text{Fe}_3\text{O}_4@\text{C}$ (b); the inset in (b) is the corresponding part of the hysteresis curve (field from -100 to 100 Oe). (c) Interaction mode of thiophene with the carboxyl groups on the surface of the $\text{Fe}_3\text{O}_4@\text{C}$. The atoms are colored as white (H), gray (C), red (O), and yellow (S). (d) Schematic illustration of the magnetic alignment process of the as-deposited $\text{Fe}_3\text{O}_4@\text{C}$ /PBTTT composite film on the substrate.

According to previous studies, because of the magnetic dipole attraction and electrostatic repulsion between particles, one dimensional (1D) chain-like structures based on these superparamagnetic colloidal nanoparticles are formed due to the induction of an external magnetic field [28,34,42,43], which can be distinctly observed in POM and AFM images. The FT-IR spectrum shows the presence of carboxyl groups on the surface of the samples. Previous research has proved that the sulfur atom of the thiophene rings and the hydrogen of the carboxyl group can form an intermolecular hydrogen bond (Figure 5c). The experimental study and density functional theory calculations show that the bond energy of the COOH-S hydrogen bond is as high as 25.92 kJ/mol (0.27 eV) [44–46]. Based on these studies, we infer that the kinetic process of the $\text{Fe}_3\text{O}_4@\text{C}$ -nanoparticles-assisted low-magnetic-field alignment can be partitioned into two stages (Figure 5d).

In the first stage, the Fe_3O_4 nanospheres in the mixed solution are quickly self-assembled into 1D chain-like structures induced by the external magnetic field and highly oriented in the direction of the magnetic field. In the second stage, the randomly dispersed PBTTT molecules in the composite solution are held in the surface of $\text{Fe}_3\text{O}_4@\text{C}$ chains by intermolecular COOH-S hydrogen bond, i.e., the backbone chains of PBTTT molecules are highly oriented by the $\text{Fe}_3\text{O}_4@\text{C}$ chains. As the solvent evaporates, molecular deposition eventually leads to the formation of macroscopically aligned films. In summary, the rapid magnetically induced self-assembly characteristic of $\text{Fe}_3\text{O}_4@\text{C}$ and its synergetic interaction with the polymer chains are key to new methods for preparing oriented thin films.

4. Conclusions

In summary, we successfully demonstrated a low-cost, upscalable, and simple magnetic alignment method by applying a low magnetic field to produce aligned semiconductor polymers film with assisted by $\text{Fe}_3\text{O}_4@\text{C}$ nanoparticles. The UV–vis and AFM data show that the chain backbones of PBTTT are preferentially aligned with the magnetic field direction. The aligned microstructure of the composite films leads to enhanced charge carrier mobility along the magnetic field direction. We can expect great potential to further improve mobility by optimizing the polymer chain alignment technique. Moreover, the degree of chain alignment of the composite films is higher than that of the pure polymer films aligned by a high magnetic field. A mechanism for nanoparticles-assisted magnetic alignment is proposed, in which the aligned $\text{Fe}_3\text{O}_4@\text{C}$ chain-like structures can effectively induce the orientation of polymer chains through intermolecular hydrogen bonds. We

believe that the strategy and methodology proposed here can also potentially be applied to other types of polymers to increase the overall performance of future sophisticated organic electronics.

Supplementary Materials: The following are available online at <https://www.mdpi.com/article/10.3390/magnetochemistry8060064/s1>. Figure S1: The photograph of the magnet (0.12 T); Figure S2: The XRD pattern of the Fe₃O₄@C nanoparticles; Figure S3: The POM images of the magnetically aligned pure PBTTT film; The red arrows denote the magnetic field direction; Figure S4: Output curves of the OFET devices of the magnetically aligned Fe₃O₄@C/PBTTT composite film with channel current perpendicular to magnetic field direction (a), unaligned spin-coated pure PBTTT film (b) and spin-coated Fe₃O₄@C/PBTTT composite film (c), respectively.

Author Contributions: Data curation, resources, methodology and writing original draft preparation, D.H.; formal analysis, validation, and supervision, T.L.; visualization, project administration, C.Y.; funding acquisition, writing—review and editing, G.P. All authors have read and agreed to the published version of the manuscript.

Funding: This work was supported financially by the Natural Science Foundation of Anhui Province (Grant 2008085QE212).

Institutional Review Board Statement: Not applicable.

Informed Consent Statement: Not applicable.

Data Availability Statement: Not applicable.

Acknowledgments: Special thanks to Hefei Hongzhong Science & Technology Company for designing and manufacturing the magnet.

Conflicts of Interest: The authors declare no conflict of interest.

References

1. Li, Q.Y.; Yao, Z.F.; Lu, Y.; Zhang, S.; Ahmad, Z.; Wang, J.Y.; Gu, X.; Pei, J. Achieving High Alignment of Conjugated Polymers by Controlled Dip-Coating. *Adv. Electron. Mater.* **2020**, *6*, 2000080. [[CrossRef](#)]
2. Gamage, P.L.; Udamulle Gedara, C.M.; Gunawardhana, R.; Bulumulla, C.; Ma, Z.; Shrivastava, A.; Biewer, M.C.; Stefan, M.C. Enhancement in Charge Carrier Mobility by Using Furans as Spacer in Thieno[3,2-b]Pyrrole and Alkylated-Diketopyrrolopyrrole Based Conjugated Copolymers. *Appl. Sci.* **2022**, *12*, 3150. [[CrossRef](#)]
3. Bae, E.J.; Kang, S.W.; Choi, G.S.; Jang, E.B.; Baek, D.H.; Ju, B.K.; Park, Y.W. Enhanced Light Extraction from Organic Light-Emitting Diodes with Micro-Nano Hybrid Structure. *Nanomaterials* **2022**, *12*, 1266. [[CrossRef](#)]
4. Dhbaibi, K.; Abella, L.; Meunier-Della-Gatta, S.; Roisnel, T.; Vanthuyne, N.; Jamoussi, B.; Pieters, G.; Racine, B.; Quesnel, E.; Autschbach, J.; et al. Achieving high circularly polarized luminescence with push-pull helicenic systems: From rationalized design to top-emission CP-OLED applications. *Chem. Sci.* **2021**, *12*, 5522–5533. [[CrossRef](#)]
5. Diterlizzi, M.; Ferretti, A.M.; Scavia, G.; Sorrentino, R.; Luzzati, S.; Boccia, A.C.; Scamporrino, A.A.; Po, R.; Quadri, E.; Zappia, S.; et al. Amphiphilic PTB7-Based Rod-Coil Block Copolymer for Water-Processable Nanoparticles as an Active Layer for Sustainable Organic Photovoltaic: A Case Study. *Polymers* **2022**, *14*, 1588. [[CrossRef](#)]
6. Vuk, D.; Radovanovic-Peric, F.; Mandic, V.; Lovrinevic, V.; Rath, T.; Panzic, I.; Le-Cunff, J. Synthesis and Nanoarchitectonics of Novel Squaraine Derivatives for Organic Photovoltaic Devices. *Nanomaterials* **2022**, *12*, 1206. [[CrossRef](#)]
7. Chang, M.; Lim, G.T.; Park, B.; Reichmanis, E. Control of Molecular Ordering, Alignment, and Charge Transport in Solution-Processed Conjugated Polymer Thin Films. *Polymers* **2017**, *9*, 212. [[CrossRef](#)]
8. Lin, F.J.; Guo, C.; Chuang, W.T.; Wang, C.L.; Wang, Q.; Liu, H.; Hsu, C.S.; Jiang, L. Directional Solution Coating by the Chinese Brush: A Facile Approach to Improving Molecular Alignment for High-Performance Polymer TFTs. *Adv. Mater.* **2017**, *29*, 1606987. [[CrossRef](#)]
9. Tanigaki, N.; Takechi, C.; Nagamatsu, S.; Mizokuro, T.; Yoshida, Y. Oriented Thin Films of Insoluble Polythiophene Prepared by the Friction Transfer Technique. *Polymers* **2021**, *13*, 2393. [[CrossRef](#)]
10. Kim, D.; Yoon, M.; Lee, J. Enhanced Performance of Cyclopentadithiophene-Based Donor-Acceptor-Type Semiconducting Copolymer Transistors Obtained by a Wire Bar-Coating Method. *Polymers* **2021**, *14*, 2. [[CrossRef](#)]
11. Yuan, Y.; Giri, G.; Ayzner, A.L.; Zoombelt, A.P.; Mannsfeld, S.C.; Chen, J.; Nordlund, D.; Toney, M.F.; Huang, J.; Bao, Z. Ultra-high mobility transparent organic thin film transistors grown by an off-centre spin-coating method. *Nat. Commun.* **2014**, *5*, 3005. [[CrossRef](#)]
12. Kim, N.-K.; Shin, E.-S.; Noh, Y.-Y.; Kim, D.-Y. A selection rule of solvent for highly aligned diketopyrrolopyrrole-based conjugated polymer film for high performance organic field-effect transistors. *Org. Electron.* **2018**, *55*, 6–14. [[CrossRef](#)]

13. Khim, D.; Han, H.; Baeg, K.J.; Kim, J.; Kwak, S.W.; Kim, D.Y.; Noh, Y.Y. Simple bar-coating process for large-area, high-performance organic field-effect transistors and ambipolar complementary integrated circuits. *Adv. Mater.* **2013**, *25*, 4302–4308. [[CrossRef](#)]
14. Jiang, Y.; Chen, J.; Sun, Y.; Li, Q.; Cai, Z.; Li, J.; Guo, Y.; Hu, W.; Liu, Y. Fast Deposition of Aligning Edge-On Polymers for High-Mobility Ambipolar Transistors. *Adv. Mater.* **2019**, *31*, e1805761. [[CrossRef](#)]
15. Xiao, M.; Kang, B.; Lee, S.B.; Perdigao, L.M.A.; Luci, A.; Warr, D.A.; Senanayak, S.P.; Nikolka, M.; Statz, M.; Wu, Y.; et al. Anisotropy of Charge Transport in a Uniaxially Aligned Fused Electron-Deficient Polymer Processed by Solution Shear Coating. *Adv. Mater.* **2020**, *32*, e2000063. [[CrossRef](#)]
16. Kim, G.W.; Kwon, E.H.; Kim, M.; Park, Y.D. Uniform and Reliable Dip-Coated Conjugated Polymers for Organic Transistors as Obtained by Solvent Vapor Annealing. *J. Phys. Chem. C* **2019**, *123*, 23255–23263. [[CrossRef](#)]
17. Kakade, M.V.; Givens, S.; Gardner, K.; Lee, K.H.; Chase, D.B.; Rabolt, J.F. Electric field induced orientation of polymer chains in macroscopically aligned electrospun polymer nanofibers. *J. Am. Chem. Soc.* **2007**, *129*, 2777–2782. [[CrossRef](#)]
18. Gupta, P.; Rajput, M.; Singla, N.; Kumar, V.; Lahiri, D. Electric field and current assisted alignment of CNT inside polymer matrix and its effects on electrical and mechanical properties. *Polymer* **2016**, *89*, 119–127. [[CrossRef](#)]
19. Winkler, A.; Modler, N.; Gude, M.; Xu, Y.; Helwig, M.; Dohmen, E.; Dittes, A.; Hohlich, D.; Lampke, T. Numerical Investigation of the Orientability of Single Reinforcement Fibers in Polymer Matrices. *Polymers* **2022**, *14*, 534. [[CrossRef](#)]
20. Mishra, S.; Bhowmick, D. Asymmetric Magnetochemistry: An Efficient Method to Grow Enantiopure Self-Assemble Monolayer. *Magnetochemistry* **2020**, *6*, 37. [[CrossRef](#)]
21. van Essen, M.; Montree, E.; Houben, M.; Borneman, Z.; Nijmeijer, K. Magnetically Aligned and Enriched Pathways of Zeolitic Imidazolate Framework 8 in Matrimid Mixed Matrix Membranes for Enhanced CO₂ Permeability. *Membranes* **2020**, *10*, 155. [[CrossRef](#)]
22. Kimura, T. Study on the effect of magnetic fields on polymeric materials and its application. *Polym. J.* **2003**, *35*, 823–843. [[CrossRef](#)]
23. Yamato, M.; Aoki, H.; Kimura, T.; Yamamoto, I.; Ishikawa, F.; Yamaguchi, M.; Tobita, M. Determination of anisotropic diamagnetic susceptibility of polymeric fibers suspended in liquid. *Jpn. J. Appl. Phys.* **2001**, *40*, 2237–2240. [[CrossRef](#)]
24. Song, G.; Kimura, F.; Kimura, T.; Piao, G. Orientational Distribution of Cellulose Nanocrystals in a Cellulose Whisker as Studied by Diamagnetic Anisotropy. *Macromolecules* **2013**, *46*, 8957–8963. [[CrossRef](#)]
25. Zaric, S.; Ostojic, G.N.; Kono, J.; Shaver, J.; Moore, V.C.; Strano, M.S.; Hauge, R.H.; Smalley, R.E.; Wei, X. Optical signatures of the Aharonov-Bohm phase in single-walled carbon nanotubes. *Science* **2004**, *304*, 1129–1131. [[CrossRef](#)]
26. Pan, G.; Chen, F.; Hu, L.; Zhang, K.; Dai, J.; Zhang, F. Effective Controlling of Film Texture and Carrier Transport of a High-Performance Polymeric Semiconductor by Magnetic Alignment. *Adv. Funct. Mater.* **2015**, *25*, 5126–5133. [[CrossRef](#)]
27. Pan, G.; Hu, L.; Su, S.; Yuan, J.; Li, T.; Xiao, X.; Chen, Q.; Zhang, F. Solvent Vapor-Assisted Magnetic Manipulation of Molecular Orientation and Carrier Transport of Semiconducting Polymers. *ACS Appl. Mater. Interfaces* **2020**, *12*, 29487–29496. [[CrossRef](#)]
28. Liu, Y.; Zhou, L.; Hu, Y.; Guo, C.; Qian, H.; Zhang, F.; Lou, X.W. Magnetic-field induced formation of 1D Fe₃O₄/C/CdS coaxial nanochains as highly efficient and reusable photocatalysts for water treatment. *J. Mater. Chem.* **2011**, *21*, 18359–18364. [[CrossRef](#)]
29. Erb, R.M.; Libanori, R.; Rothfuchs, N.; Studart, A.R. Composites reinforced in three dimensions by using low magnetic fields. *Science* **2012**, *335*, 199–204. [[CrossRef](#)]
30. Billaud, J.; Bouville, F.; Magrini, T.; Villevieille, C.; Studart, A.R. Magnetically aligned graphite electrodes for high-rate performance Li-ion batteries. *Nat. Energy* **2016**, *1*, 16097. [[CrossRef](#)]
31. Genorio, B.; Peng, Z.W.; Lu, W.; Hoelscher, B.K.P.; Novosel, B.; Tour, J.M. Synthesis of Dispersible Ferromagnetic Graphene Nanoribbon Stacks with Enhanced Electrical Percolation Properties in a Magnetic Field. *Acs Nano* **2012**, *6*, 10396–10404. [[CrossRef](#)] [[PubMed](#)]
32. Hekmatara, H.; Seifi, M.; Forooraghi, K. Microwave absorption property of aligned MWCNT/Fe₃O₄. *J. Magn. Mater.* **2013**, *346*, 186–191. [[CrossRef](#)]
33. Hu, H.; Chen, Q.-W.; Cheng, K.; Tang, J. Visually readable and highly stable self-display photonic humidity sensor. *J. Mater. Chem.* **2012**, *22*, 1021–1027. [[CrossRef](#)]
34. Hu, H.; Chen, Q.-W.; Wang, H.; Li, R.; Zhong, W. Reusable photonic wordpad with water as ink prepared by radical polymerization. *J. Mater. Chem.* **2011**, *21*, 13062–13067. [[CrossRef](#)]
35. Liu, J.; Dong, S.; He, Q.; Yang, S.; Xie, M.; Deng, P.; Xia, Y.; Li, G. Facile Preparation of Fe₃O₄/C Nanocomposite and Its Application for Cost-Effective and Sensitive Detection of Tryptophan. *Biomolecules* **2019**, *9*, 245. [[CrossRef](#)]
36. Tran, T.V.; Phan, T.-Q.T.; Nguyen, D.T.C.; Nguyen, T.T.; Nguyen, D.H.; Vo, D.-V.N.; Bach, L.G.; Nguyen, T.D. Recyclable Fe₃O₄@C nanocomposite as potential adsorbent for a wide range of organic dyes and simulated hospital effluents. *Environ. Technol. Innov.* **2020**, *20*, 101122. [[CrossRef](#)]
37. Ghereghlou, M.; Esmaili, A.A.; Darroudi, M. Preparation of Fe₃O₄@C-dots as a recyclable magnetic nanocatalyst using *Elaeagnus angustifolia* and its application for the green synthesis of formamidines. *Appl. Organomet. Chem.* **2021**, *35*, e6387. [[CrossRef](#)]
38. Soeda, J.; Matsui, H.; Okamoto, T.; Osaka, I.; Takimiya, K.; Takeya, J. Highly oriented polymer semiconductor films compressed at the surface of ionic liquids for high-performance polymeric organic field-effect transistors. *Adv. Mater.* **2014**, *26*, 6430–6435. [[CrossRef](#)]
39. Biniek, L.; Leclerc, N.; Heiser, T.; Bechara, R.; Brinkmann, M. Large Scale Alignment and Charge Transport Anisotropy of pBTTT Films Oriented by High Temperature Rubbing. *Macromolecules* **2013**, *46*, 4014–4023. [[CrossRef](#)]

40. Lee, M.J.; Gupta, D.; Zhao, N.; Heeney, M.; McCulloch, I.; Sringhaus, H. Anisotropy of Charge Transport in a Uniaxially Aligned and Chain-Extended, High-Mobility, Conjugated Polymer Semiconductor. *Adv. Funct. Mater.* **2011**, *21*, 932–940. [[CrossRef](#)]
41. Schott, S.; Gann, E.; Thomsen, L.; Jung, S.H.; Lee, J.K.; McNeill, C.R.; Sringhaus, H. Charge-Transport Anisotropy in a Uniaxially Aligned Diketopyrrolopyrrole-Based Copolymer. *Adv. Mater.* **2015**, *27*, 7356–7364. [[CrossRef](#)]
42. Guo, C.; Lu, W.; Wei, G.; Jiang, L.; Yu, Y.; Hu, Y. Formation of 1D chain-like Fe₃O₄@C/Pt sandwich nanocomposites and their magnetically recyclable catalytic property. *Appl. Surf. Sci.* **2018**, *457*, 1136–1141. [[CrossRef](#)]
43. Shang, S.; Liu, Z.; Zhang, Q.; Wang, H.; Li, Y. Facile fabrication of a magnetically induced structurally colored fiber and its strain-responsive properties. *J. Mater. Chem. A Mater.* **2015**, *3*, 11093–11097. [[CrossRef](#)]
44. Pishevarz, G.; Erfan-Niya, H.; Zaminpayma, E. The role of hydrogen bonding in interaction energy at the interface of conductive polymers and modified graphene-based nanosheets: A reactive molecular dynamics study. *Comput. Mater. Sci.* **2018**, *155*, 499–523. [[CrossRef](#)]
45. Wu, L.; Sitamraju, S.; Xiao, J.; Liu, B.; Li, Z.; Janik, M.J.; Song, C. Effect of liquid-phase O₃ oxidation of activated carbon on the adsorption of thiophene. *Chem. Eng. J.* **2014**, *242*, 211–219. [[CrossRef](#)]
46. Lane, J.R.; Hansen, A.S.; Mackeprang, K.; Kjaergaard, H.G. Kinetic Energy Density as a Predictor of Hydrogen-Bonded OH-Stretching Frequencies. *J. Phys. Chem. A* **2017**, *121*, 3452–3460. [[CrossRef](#)]